ESTIMATING THE ATMOSPHERIC PATH RADIANCE COMPONENT IN HYPERSPECTRAL IMAGERY OVER SHALLOW COASTAL REGIONS USING A SINGLE-SCATTERING MODEL AND IN SITU DERIVED TWO-WAY DIFFUSE ATTENUATION COEFFICIENTS

Bruce C. Monger[1], David D. R. Kohler[2] and William D. Philpot[2],
1. Ocean Resources and Ecosystems Program, Center for the Environment,
4134 Snee Hall, Cornell University, Ithaca NY 14853,
2. School of Civil and Environmental Engineering, Cornell University
453 Hollister Hall, Ithaca, NY14853

INTRODUCTION

Atmospheric correction of remote sensing imagery in optically shallow waters remains a challenge. The difficulty stems from the need to select an appropriate atmospheric model that is based on the proportion of marine and terrestrial aerosols present in a particular scene. This problem is further complicated by contributions of bottom reflection and the fact that coastal waters may not be perfectly absorbing in the near infrared. An established solution to this problem is to perform calibrations based on a small number of fixed points where directly measured water leaving radiance measurements are compared with remotely sensed estimates at precisely the same locations (Hooker and McClain 2000, McClain et al. 1998).

Small navigation errors in remote sensing imagery can lead to large errors in calibration, especially in regions exhibiting strong gradients in depth or heterogeneous bottom types. As an alternative approach, we have developed a method for determining atmospheric path radiance in remotely sensed imagery that utilizes a single-scattering model fed by in situ measurements. With the single assumption of a locally uniform in-water diffuse attenuation coefficient, we are able to estimate atmospheric path radiance over regions of constant bottom type based on deviations between model prediction and remotely observed changes in radiance that occur with changes in bottom depth. This approach greatly enhances the number of observation points used to determine atmospheric path radiance over finite regions within an image.

To test our ability to extract atmospheric path radiance from the total radiance signal, we used synthetically derived water leaving radiance values for different depths and then systematically added increasingly greater levels of atmospheric path radiance to obtain a total (water + atmosphere) radiance signal. We then tested how well the atmospheric path radiance could be recovered from the total signal. The expectation is that once the formulations and computer algorithms are fully validated with synthetic data, the approach will be directly applicable to raw hyperspectral image data.

THEORETICAL BACKGROUND

Research aimed at understanding how environmental variability in optically shallow waters affects radiances measured by a remote detector often begins with a single-scattering model of the form:

$$L_d = L_b e^{-gz} + L_\infty , \quad (1)$$

where L_d = radiance observed at the remote detector
g = an effective attenuation coefficient
z = water depth
L_b = a radiance term that is sensitive to bottom reflectance
L_∞ = radiance observed in optically deep water ($gz \rightarrow \infty$)

All terms, except for depth, are wavelength dependent. In this paper the formulation of Equation 1 is derived from the Single Scattering Irradiance (SSI) model (Philpot, 1987), and assumes that the optical properties of the water are vertically homogeneous. The SSI model is a simplified two-flow model based on irradiance. The assumption of vertical homogeneity is not always realistic, but serves as a reasonable starting point. The second assumption can be avoided if a full radiative transfer model is used (e.g., Hydrolight Software, Sequoia Scientific Inc.). The variable, g, should not be confused with the downwelling diffuse attenuation coefficient (k_d) integrated over depth (Philpot, 1987). The two variables are related by:

$$g = k_d + aD_u \quad (2)$$

where: a is the absorption coefficient, and D_u is the distribution function for upwelling irradiance (Preisendorfer, 1976). L_b will depend on the relative difference between the bottom reflectance and the water reflectance (Philpot 1989).

Equation 1 can be modified to account for the diffuse transmittance and path radiance, associated with scattering and absorption by the atmosphere, to yield an expression of the form:

$$L_d = \tau L_b e^{-gz} + \tau L_\infty + L_* , \quad (3)$$

where τ = atmospheric transmittance
L_* = atmospheric path radiance

Both τ and L_* are wavelength dependent. This Formulation of the atmospheric contribution is an approximation to the full radiative transfer process, but is commonly used as a good first-order approximation.

If we assume for the moment that $\tau = 1.0$, then Equation 3 may be rewritten in the form:

$$(L'_d - L_*) = L_b e^{-gz} \quad (4)$$

where $L'_d = (L_d - L_\infty)$.

For two different locations (denoted by the subscripts i, j) of distinctly different water depth the following ratio holds

$$(L'_{di} - L_*)/(L'_{dj} - L_*) = L_{bi} e^{-gzi} / L_{bj} e^{-gzj}. \quad (5)$$

If bottom type and atmospheric contribution are assumed to be constant over the region of interest, Equation 5 can be rewritten, after also taking logarithms of both sides, as:

$$[ln(L'_{dj} - L_*) - ln(L'_{di} - L_*)]/g = \Delta z_{i,j} \quad (6)$$

where $\Delta z_{i,j}$ is the depth change between locations i and j in the remotely sensed image. It is important to note that if $L_* = 0$, then under present model assumptions the magnitude of $\Delta z_{i,j}$ must be the same for all spectral bands. This basic fact can be used to determine the magnitude and spectral shape of L_* for the more realistic case where L_* is not equal to zero. The magnitude and spectral shape of L_* is found by selecting a finite number of L'_d estimates over a region in a hyperspectral image where bottom type is known to be constant, depth varies significantly, and in the vicinity of where the value for g and consequently L_∞, has been determined via in situ measurements. For n selected depths, there will be $N=\sum_{i=2,n}$ (i-1) total Δz permutations and consequently N expressions of the form given by Equation 6. Constrained minimization techniques can then be used to determine the magnitude and spectral shape of L_* that minimizes the band-to-band variance of all possible $\Delta z_{i,j}$ permutations.

METHODS

To examine the feasibility of accurately recovering L_* from hyperspectral data contaminated with atmospheric effects, we used a synthetic data set comprised of L'_d estimates for different depths and varying levels of L_*. Using this synthetic data we then attempted to recover L_* for different scenarios of increasing contributions of L_* relative to L'_d. The solutions were then compared with the known additions of L_* to determine the accuracy and precision of the computational method.

Synthetic values of L'_d were derived with the aid of Hydrolight 4.0 software (Mobley, 1998). The software's default water column type and predefined bottom-type spectral characteristics for sandy bottom were used in the present study. Further details concerning Hydrolight modeling are presented by Kohler (1999). The resulting g and L_b values are given in Figures 1a,b. L_d values were determined for the depths: 2.0, 3.5, 5.0, 7.0 and 10.0 m (Fig. 1c). L_∞ was approximated by determining L_d for a water depth of 50 m (Fig. 1c). The spectral range for Hydrolight generated data was between 350 and 700 nm and the spectral resolution was 10 nm.

A spectral shape of L_* was derived by normalizing the tabulated path radiance data given by Kok (1972, Table 1). The shape of L_* was kept constant while the magnitude was varied sequentially from relatively low atmospheric contributions to the total radiance signal (< 5.0% of the total radiance) to relatively high atmospheric contributions (> 95% of the total radiance). Twenty different levels of L_* were tested, however, for purposes of clearer graphical presentation, the results for just four path radiance levels, spanning the full range examined, are presented in the current paper. The different levels of L_* used in this study are presented in Figure 2.

Selecting 5 distinct depths in the current analysis yields 10 $\Delta z_{i,j}$ permutations and therefore 10 equations of the form given by Equation 6. The goal is then to determine the value of L_* that yields the lowest possible spectral variance for Δz over all ten $\Delta z_{i,j}$ permutations. This was done for each level of L_* examined. The minimization problem was determined using a procedure that solves nonlinear optimization problems based on an implemented of the GRG algorithm supplied by Windward Technologies (http://web.wt.net). The procedure was accessed using a standard IDL 5.3 software (Research Systems Inc.) function called CONSTRAINED_MIN. Finding the global

minimum in the total Δz variance is highly sensitive to the initial guess of L_*. Consequently, a rather elaborate programming scheme was developed to systematically vary the initial guess for L_* over the fullest possible range (0.1 to 0.99 of total radiance signal: $L'_d + L_*$). A total of 1,200 initial guesses were tried for each level L_* tested. The complete IDL code used to generate the solutions is available upon request.

RESULTS

The magnitude and spectral shape of L_* that was recovered from the total radiance is presented in Figure 3 along with the true levels of L_* that were initially added to L'_d. It was always possible to recover the initial L_* spectra with very high precision over the full range of L_* levels tested. There was a small (< 0.4 mW m^{-2} nm^{-1}) but detectable spectral bias in the L_* solutions (Fig. 4). This bias was persistent for all L_* levels tested with an RMS error of about 0.0002 mW m^{-2} nm^{-1}.

Estimated values of bottom depth change are given in Figure 5. There were generally good recoveries of Δz. for all conditions tested. The precision of the Δz estimates between different levels of L_* addition matched the very high precision found in the L_* recoveries given above. There was, however an obvious bias in the estimated Δz that did not depend on the level of L_* addition, but did depend on the depth ranges being examined (Fig. 6). Best estimates (within 2% of actual depth changes) were obtained for the shallowest waters with small depth change. Poorest estimates (> 35% error) were obtained for the deepest waters and largest depth changes.

DISCUSSION AND CONCLUSIONS

The results presented in this study demonstrate a novel new approach for estimating L_* in regions where g and L_∞ have been directly measured. Assuming g and L_∞ to be horizontally homogeneous, one can predict how L'_d must change with changing bottom depths in local subregions of constant bottom type. Any deviations in the expected change in L'_d can be attributed to L_* and using the optimization scheme outlined in this paper it is possible to determine the shape and magnitude of L_* with very high precision and small bias. This approach was shown to be highly robust in that it was able to recover L_* from the total radiance over a range of L_* contributions that extend from a 10% to 95% of the total radiance measured by the sensor. Additionally, this approach yields reasonably good estimates of Δz.

The great advantage of this approach is that accurate geo-referencing of hyperspectral imagery is less important. This approach will be most useful for situations where bottom depth varies greatly while water type exhibits little horizontal change. Moreover, the sample size can be greatly increased over fixed station validation methods. The added sample size will reduce validation errors caused by signal noise found in raw hyperspectral image data.

While precision in the estimates L_* and Δz were very small over the full range of L_* additions tested, there was a measurable bias in both estimates. The bias in the recovered L_* relative to the known L_* was very small (Fig. 4) and was likely due to subtle spectral discrepancies between L_* derived from the single-scattering model (Eq. 1) and L_*

derived from the full radiative transfer solutions generated with the Hydrolight simulations. L'_d spectra derived from Hydrolight simulation and the single-scattering model are presented in Figure 7. The spectral discrepancies range from + 2.0 to –1.0 mW m^{-2} nm^{-1} and so it seems reasonable to assume the spectral bias in the L_* solutions was a result of the small spectral differences between Hydrolight simulated and modeled L'_d.

Small spectral differences in Hydrolight simulated data and the single-scattering model are also the likely cause of the biases in the Δz estimates. Shown in Figure 5 are the Δz estimates derived for varying amounts of added L_* and also for the case where L_* is zero. The pattern of bias in the Δz estimate without L_* additions followed closely the pattern exhibited for the cases where L_* was present. A similar pattern of error was found in depth estimates presented by Philpot (1989, Fig., 10). This demonstrates that Δz estimates were probably caused by the underlying assumptions of the single-scattering model rather than by errors in the solution algorithm described in this paper.

This paper describes a promising new method for extracting L_* from raw hyperspectral imagery. However, it has not addressed the issue of determining τ. Work by our group is currently underway to develop a solution scheme very similar to the one describe in this paper that will be capable of estimating τ for cases where L_b is also known. When all work is compete, this approach will provide a useful means of making atmospheric corrections to hyperspectral imagery in optically shallow areas that have a concurrent field measurement program.

LITERATURE CITED

Hooker S. B., McClain C. R. (2000). The calibration and validation of SeaWiFS data Progr. Ocenaogr. 45:427-465

Kohler, D. D. R. (1999) Comparison of derivative based and traditional bathymetric algorithms for hyperspectral data. Master Theses, Cornell University.

Kok, C. J. (1972). Spectral irradiance of daylight at Pretoria. J. Phys. D. Appl. Phys, 5:1513-1520.

McClain, C. R., M. L. Cleave, G. C. Feldman, W. W. Gregg, S. B. Hooker, and N. Kuring. (1998). Science quality SeaWiFS data for global biosphere research. Sea Tech. 39:10-16

Mobley, C. D. (1998). Hydrolight 3.0 Users' Guide. Sequoia Scientific, Inc. Mercer Island, WA.

Philpot, W. D. (1987). Radiative Transfer in Stratified Waters: A Single-Scattering Approximation for Irradiance. Applied Optics 26:4123-4132.

Philpot, W. D. (1989). Bathymetric mapping with passive multispectral imagery. Appl. Optics 28:1569-1578.

Preisendorfer, R. W. (1976). Hydrologic Optics, Vol 5. U.S. Department of Commerce USGPO, 1976-687-487-/56 Region 8.

This research was supported by the Office of Naval Research, Environmental Optics Program, under contract N00014-97-1-0721.

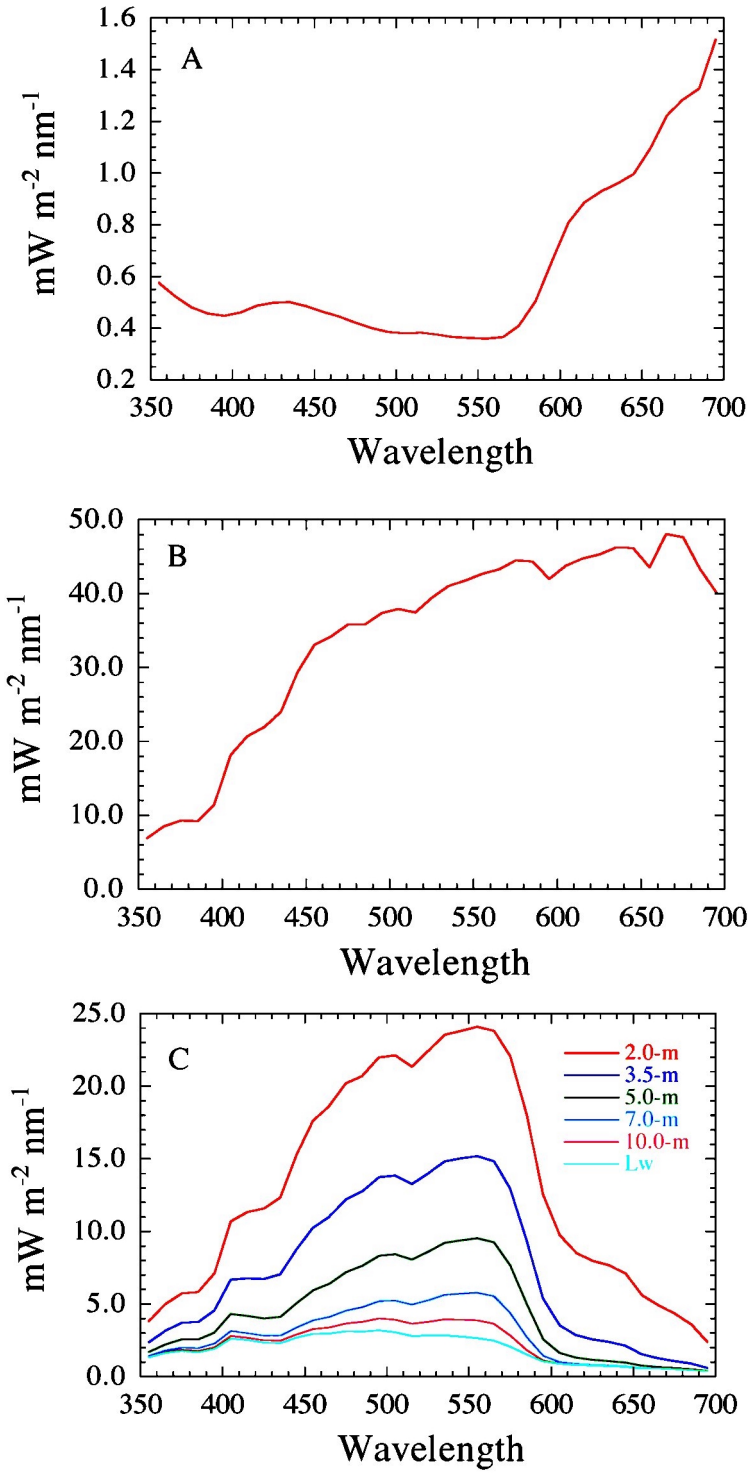

Figure 1. Synthetic data of water column optical properties used in the present study. Estimates of g, L_b and L_d, are presented in A, B and C, respectively. Spectra were generated by numerical simulation using Hydrolight 4.0 (Sequoia Inc.). See text for definitions of the spectral terms.

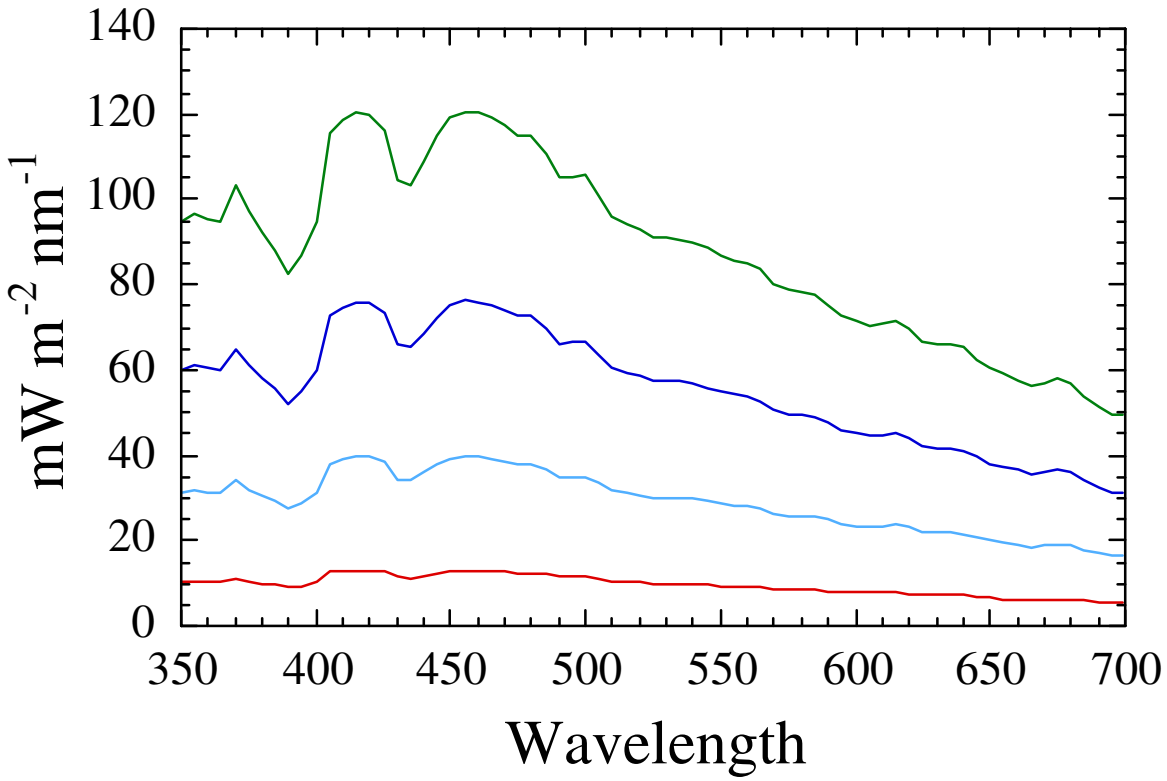

Figure 2. Four levels of L_* at were added to L'_d (Fig. 1) and subsequently recovered, using the solution algorithm described in the text.

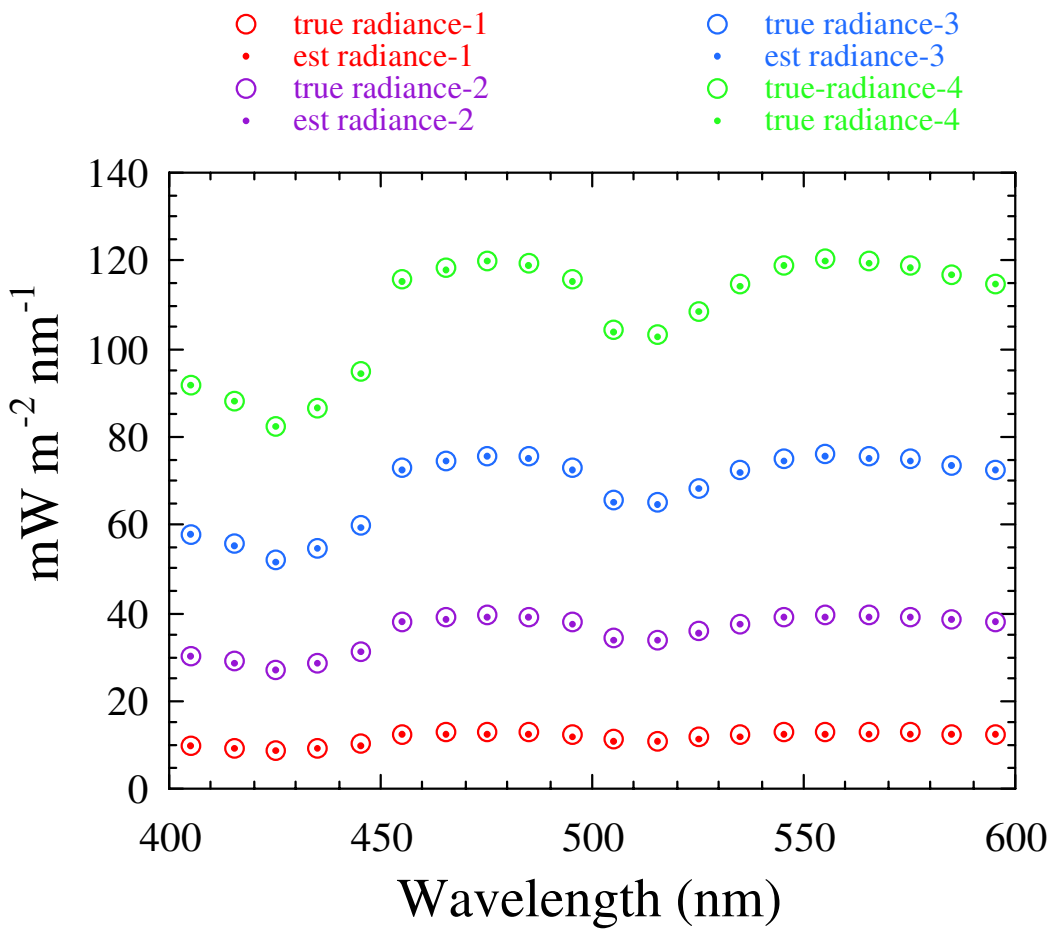

Figure 3. Spectra of L_* initially added to L'_d (large open circles) and the spectra of L_* recovered using the solution algorithm described in the text (small closed circles).

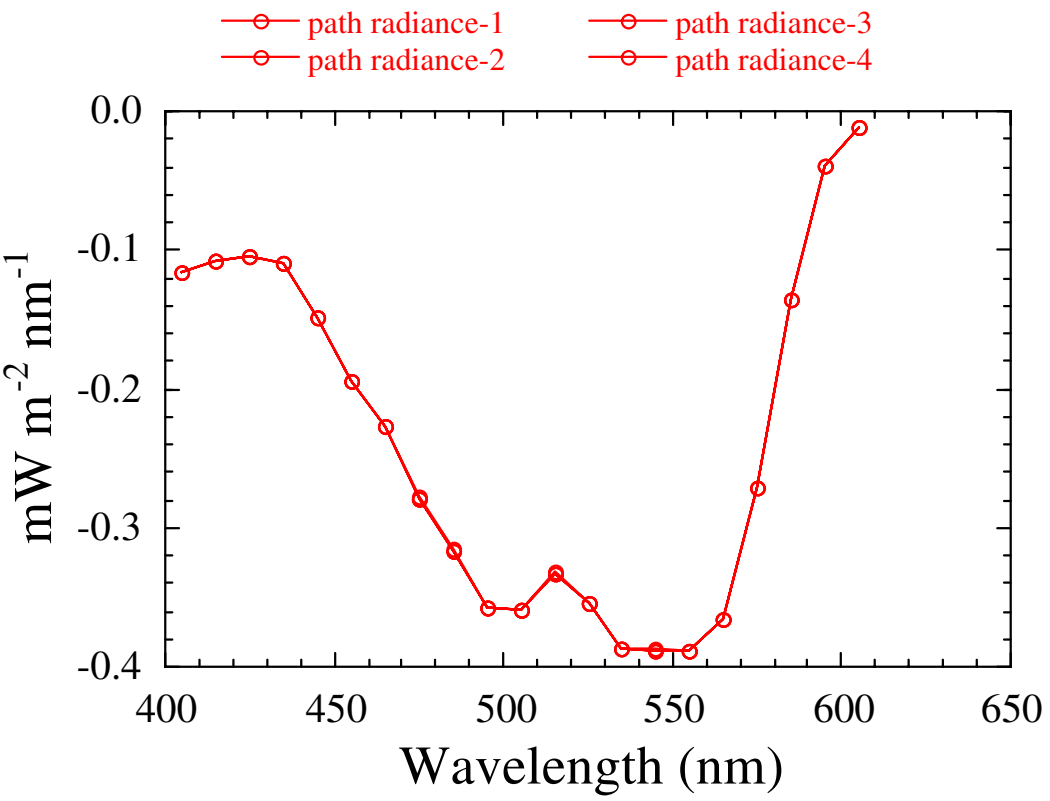

Figure 4. Residual error in the estimate of L_*, expressed as (estimated L_*) – (known L_*), for varying levels of L_* initially added to L'_d (Figs. 1, 2). RMS error between curves was less than 0.0002 mW m^{-2} nm^{-1}.

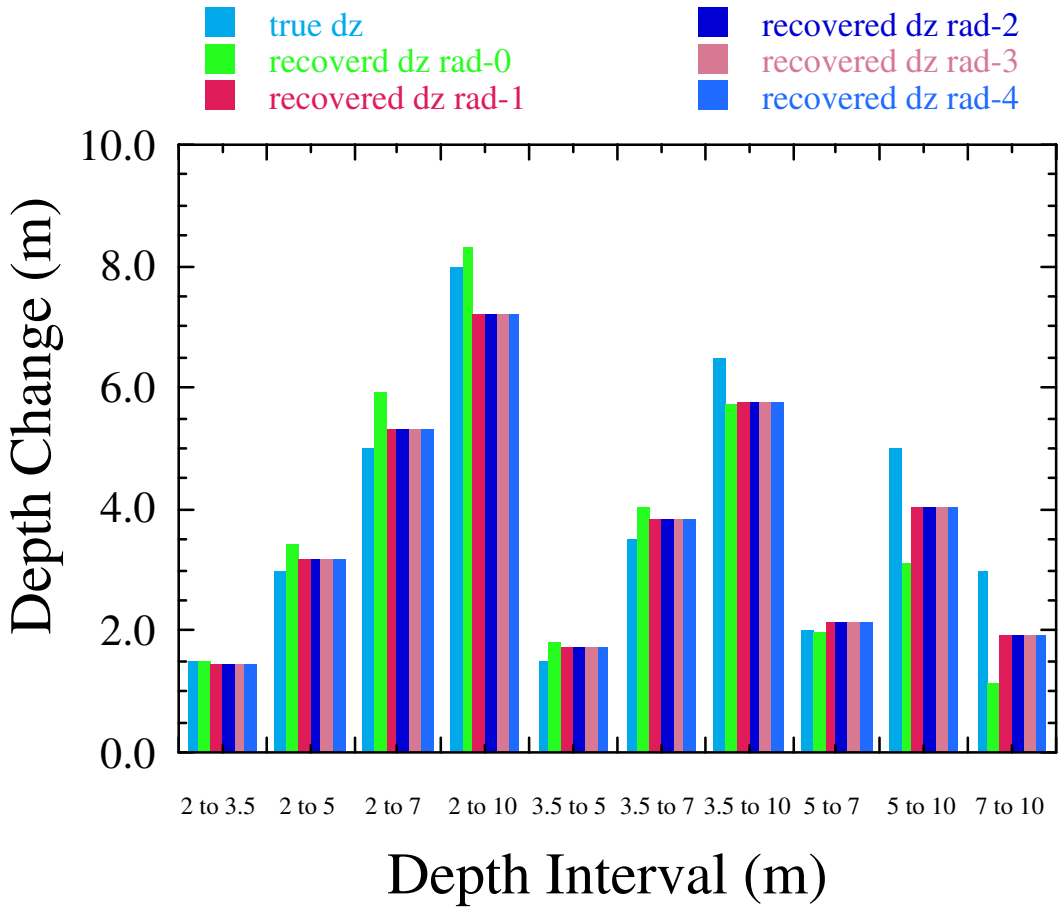

Figure 5. Estimates of depth change for all depth intervals tested under varying levels of L_* addition to L'_d (Figs. 1, 2).

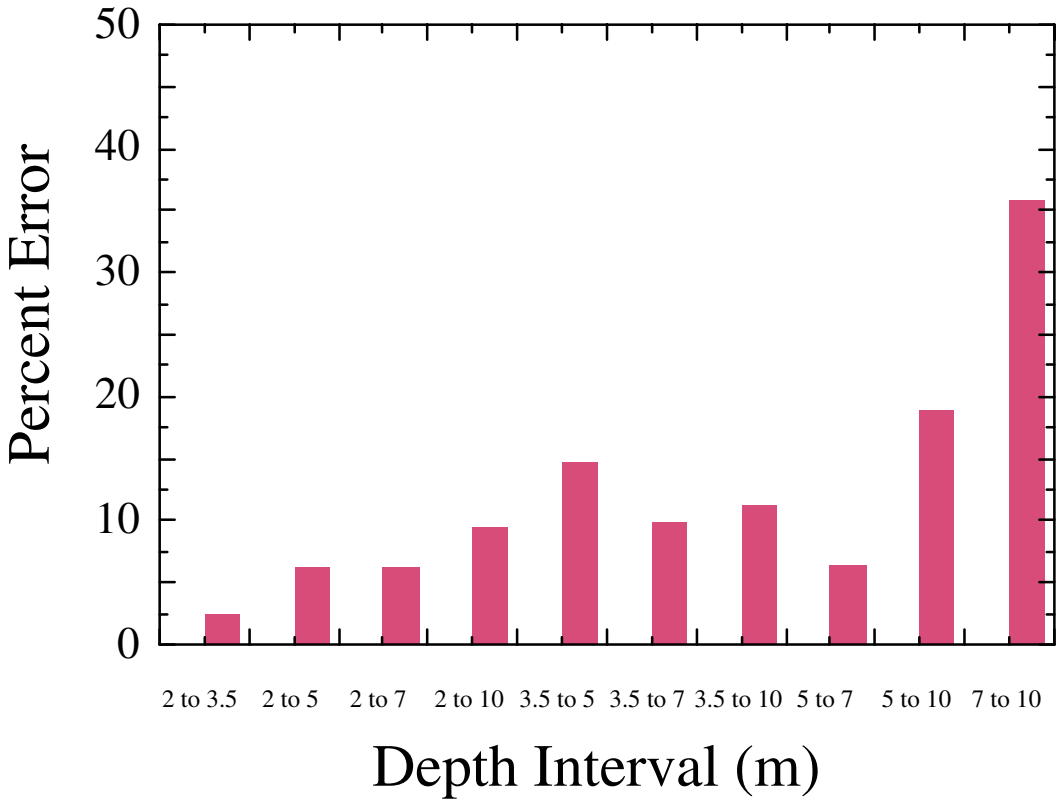

Figure 6. Percent error in depth change estimate, expressed as (estimated-Δz.-actual-Δz.)/actual-Δz, for each of the depth intervals tested. Error results were essentially the same under all four L^* conditions (all data not shown).

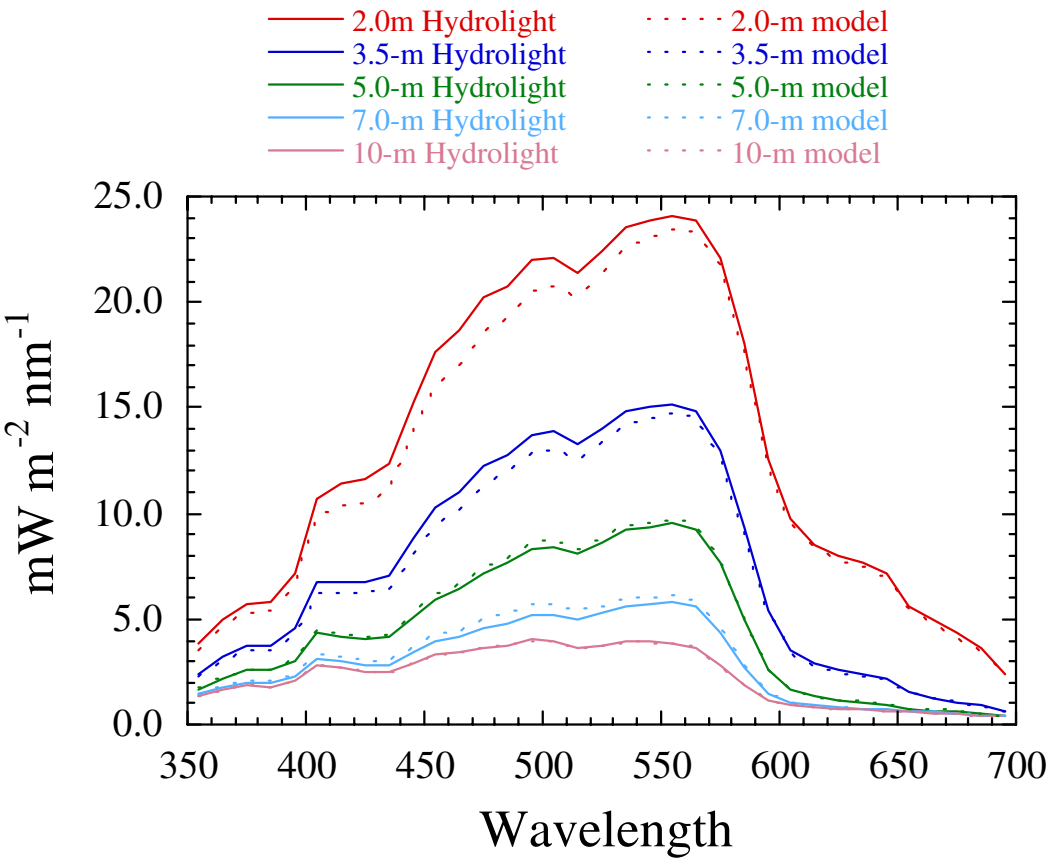

Figure 7. Spectra of L'_d determined from Hydrolight simulation (solid lines) versus L'_d generated from Eq. 1 in conjunction with g and L_b spectra presented in Fig. 1 (dashed lines).